

1 PyXRD v0.6.7: a free and open source program to quantify disordered
2 phyllosilicates using multispecimen X-ray diffraction profile fitting.

3 Mathijs Dumon^{1*}, Eric Van Ranst¹

4 ¹ Department of Geology and Soil Science (WE13), Ghent University, Krijgslaan 281/S8, B-9000 Ghent, Belgium

5

6 * Corresponding author:

7 Department of Geology and Soil Science (WE13)

8 Faculty of Sciences, Ghent University, Krijgslaan 281/S8, B-9000 Gent, Belgium

9 Phone: +32 (0)9 264 46 17

10 E-mail: mathijs.dumon@ugent.be

11

12 **Abstract**

13 This paper presents a free and open-source program called PyXRD (short for Python X-
14 ray diffraction) to improve the quantification of complex, poly-phasic mixed-layer
15 phyllosilicate assemblages. The validity of the program was checked by comparing its
16 output with Sybilla v2.2.2, which shares the same mathematical formalism. The novelty of
17 this program is the ab initio incorporation of the multispecimen method, making it possible
18 to share phases and (a selection of) their parameters across multiple specimens. PyXRD
19 thus allows modelling multiple specimens side by side, and this approach speeds up the
20 manual refinement process significantly. To check the hypothesis that this multispecimen
21 set-up – as it effectively reduces the number of parameters and increases the number of
22 observations – can also improve automatic parameter refinements, we calculated X-ray
23 diffraction patterns for four theoretical mineral assemblages. These patterns were then
24 used as input for one refinement employing the multispecimen set-up and one employing
25 the single-pattern set-ups. For all of the assemblages, PyXRD was able to reproduce or
26 approximate the input parameters with the multispecimen approach. Diverging solutions
27 only occurred in single-pattern set-ups which do not contain enough information to discern
28 all minerals present (e.g. patterns of heated samples). Assuming a correct qualitative
29 interpretation was made and a single pattern exists in which all phases are sufficiently
30 discernible, the obtained results indicate a good quantification can often be obtained with
31 just that pattern. However, these results from theoretical experiments cannot automatically
32 be extrapolated to all real-life experiments. In any case, PyXRD has proven to be useful
33 when X-ray diffraction patterns are modelled for complex mineral assemblages containing
34 mixed-layer phyllosilicates with a multispecimen approach.

35 **Keywords:** quantitative, XRD, clay mineralogy, PyXRD, multispecimen

36 **1. Introduction**

37 Clay minerals (i.e. phyllosilicates) are among the most difficult minerals to study in detail
38 due to their inherent chemical and structural variability (Środoń, 2006; Velde and Meunier,
39 2008; Hubert et al., 2012). Nonetheless, these minerals are one of the most abundant
40 constituents of the Earth's upper crust, and have an important influence on various
41 physical (e.g. plasticity, shear strength, porosity) and chemical (e.g. buffering and
42 exchange capacities, pH, electrical conductivity) properties (Agbenin and Tiessen, 1995;
43 Vernik and Liu, 1997; Righi et al., 1999; Wen and Aydin, 2003; Lado and Ben-Hur, 2004;
44 Caner et al., 2010). Phyllosilicates are also very reactive phases responding quickly to
45 changes in their environment (Pai et al., 2004; Meunier, 2007; Velde and Meunier, 2008;
46 Cornelis et al., 2014).

47 Therefore, quantitative information on the mineralogical composition of clay-bearing
48 samples is an important step in characterizing and understanding them. Different
49 techniques can be used to quantify clay minerals, but those using X-ray diffraction are the
50 most abundant and have proven to be the most reliable (Plançon, 1981; Reynolds Jr.,
51 1985; Drits and Tchoubar, 1990; Righi et al., 1999; Sakharov et al., 1999a; Środoń, 2006;
52 Hubert et al., 2009, 2012; Ufer et al., 2012a; b; Viennet et al., 2015). Programs calculating
53 X-ray diffraction patterns usually provide the highest level of detail because the input for
54 such models can be considered an approximation of the real structure of the minerals (e.g.
55 layer structures, composition, stacking parameters, interlayer composition, orientation). As
56 such, this approach does not only yield quantitative data, but also structural and
57 compositional information. However, this also means a large number of variables are
58 involved, some of which are very difficult to predict or estimate in advance. In combination
59 with the complex, poly-phasic nature of many natural samples, it is a challenge to create
60 software that allows for the quantification of clay minerals.

61 Two complementary methods exist to analyse clay minerals using X-ray diffraction. One
62 uses powder samples, for which the orientation of crystallites is considered to be
63 approximately random, and the other uses oriented samples, in which the orientation of
64 crystallites occurs mainly along a plane of preferred orientation. Originally, powder X-ray
65 diffraction was and still is used to determine crystal structures for unknown phases (not
66 just phyllosilicates), which then developed into quantitative analysis. However, for
67 disordered structures like mixed-layered clay minerals, powder patterns are often difficult
68 to interpret. In such cases oriented patterns can be used to focus on the stacking
69 (dis)order along the c^* axis. Since the 1970's, several computer programs have been
70 developed to calculate X-ray diffraction patterns for (disordered) clay minerals (Kakinoki &
71 Komura 1965; Reynolds, 1967; Ergun, 1970; Sakharov & Drits, 1973; Drits & Sakharov,
72 1976; Plançon, 1981). Examples of commonly used programs are the NEWMOD[®]-family
73 (Reynolds Jr., 1985; Pevear and Schuette, 1993; Reynolds Jr. and Reynolds III, 1996;
74 Yuan and Bish, 2010), MLM2C/3C and derivatives (Plançon and Drits, 2000), Sybilla (Aplin
75 et al., 2006; McCarty, 2015), DIFFaX (Treacy et al., 1991) and BGMN (Ufer et al., 2012a;
76 b). Some of these programs (e.g. DIFFaX, BGMN, Wildfire, Sybilla 3D) are able to
77 calculate X-ray diffraction patterns for random powder diffraction patterns, while others
78 (NEWMOD[®], MLM2C, MLM3C, Sybilla) focus only on calculating one-dimensional (00l)
79 patterns.

80 Another aspect to consider is the ability of these programs to automatically refine
81 parameters. For instance, the last version of NEWMOD[®] uses a simple linear least-
82 squares algorithm, Sybilla makes use of a genetic algorithm, and BGMN has a custom
83 least-squares algorithm. In essence, all of these algorithms try to find a solution by
84 minimizing a target function, usually a measure for the difference between the calculated
85 and observed data. This difference is usually defined as the sum of the squares of the

86 errors or as the pattern's Rp factor (Toby, 2006). A linear or ordinary least-squares
87 algorithm works well when there is a well-defined global minimum and the target function
88 is relatively smooth. However, for more complex cases this is often not the case, and as a
89 result an ordinary least-squares might not converge at all. Algorithms using a more
90 stochastic approach, like genetic algorithms, can partly overcome problems related to
91 target function smoothness or poorly defined minima (also see section 2.4). Nonetheless,
92 any algorithm will require some guidance e.g. by not releasing all parameters for automatic
93 refinement at once, by adjusting some parameters manually, by setting upper and lower
94 limits or by choosing starting values close enough to the actual solution. The reason is that
95 models describing X-ray diffraction by disordered layered minerals can not always be
96 constrained adequately, and a successful quantification is still very dependent on the skill
97 of the individual modeller. As a result, most published quantifications of complex mixed-
98 layer assemblages employ a time-consuming trial-and-error approach at some point in the
99 modelling process.

100 Several authors used a 'multispecimen approach' to further constrain their models (Drits,
101 1997; Sakharov et al., 1999a; b; Hubert et al., 2012 and references therein). This
102 approach involves recording multiple 'specimens' or patterns (e.g. air-dried, glycolated,
103 heat treatments) of the same sample and creating a structural model that can explain the
104 observed features for all patterns. The reason for doing this is that swelling layers (like
105 smectite and vermiculite layers) will expand or contract in response to these treatments.
106 The level of expansion or contraction can be related to layer charges, and helps in
107 discerning the different swelling phases present and understanding their stacking
108 (dis)order (Ferrage et al. 2005a,b; Michot et al., 2005; Ferrage et al. 2007; Dazas et al.,
109 2015). In short, this approach allows to determine the structure and type of (mixed-layer)
110 clay minerals present in the sample with higher certainty. However, today not a single

111 program allows for a side-by-side calculation of these patterns. Because of this, modellers
112 are still forced to refine their model parameters on one specimen and then check if the
113 solution also explains the other observations. As long as a manual trial-and-error
114 refinement process is used, this does not pose too many practical problems aside from the
115 time needed. In theory however, a program able to integrate all the observations and
116 calculate patterns for them could lead to better automatic parameter refinements, a
117 hypothesis tested in this paper using theoretical assemblages.

118 The program presented in this paper, called PyXRD (short for Python X-ray Diffraction),
119 was designed with this multispecimen approach in mind. It (selectively) shares phase
120 parameters across specimens and keeps phase quantities identical in each specimen,
121 thus reducing the number of parameters while at the same time increasing the number of
122 observations. Other design goals for PyXRD were (i) to have an easy-to-use interface, (ii)
123 to be an open program allowing as many aspects of the input to be changed as possible,
124 (iii) to provide a means for automatic parameter refinement, and (iv) to provide an open-
125 source program for others, allowing them to use the software freely and make
126 improvements where they see fit.

127 This paper illustrates the general structure of this program and presents the results from a
128 comparison between PyXRD and Sybilla v2.2.2 and between automatic parameter
129 refinements for several theoretical mineral assemblages, with and without the use of the
130 multispecimen approach. The software manual contains more detailed information about
131 the numerical solutions used for calculating the X-ray diffraction patterns and a guided
132 example on how to create projects using the graphical user interface (GUI).

133 **2. Materials and methods**

134 **2.1 Model implementation and licence**

135 PyXRD is written in Python 2.7 and uses a number of open-source third-party modules.
136 The GUI utilizes PyGTK as widget toolkit and has an internal model-view-controller
137 framework. To improve calculation speed, PyXRD makes use of the NumPy and SciPy
138 libraries. NumPy provides multidimensional array objects and many related routines for
139 manipulating them, while SciPy provides more complex mathematical and scientific
140 algorithms built on top of NumPy (Jones et al., 2001; van der Walt et al., 2011). The
141 Matplotlib library is used for plotting patterns and data (Hunter, 2007). Finally, the
142 Distributed Evolutionary Algorithms for Python (DEAP) library is used to harness to power
143 of evolutionary algorithms to automatically refine parameters (Fortin et al., 2012).
144 PyXRD is released under a BSD licence, except for the mvc module which, as it is a
145 derived work from the gtkmvc project, is licensed as GNU LGPL v2.

146 **2.2 Program data structure**

147 PyXRD is implemented according to a model-view-controller (mvc) paradigm separating
148 data and calculations from GUI-related aspects. In the following section, an overview is
149 given of the most important objects found in the data layer and their associations. More
150 details can also be found in the manual and the source code documentation.

151 **Project object**

152 The user interface of PyXRD can create (or load) a single *Project* object. It is a container
153 object grouping lists of *AtomType*, *Phase*, *Specimen* and *Mixture* objects together. These
154 are the four top-level objects which are used to calculate X-ray diffraction patterns. Their
155 associations are shown schematically in figure 1. The purpose of each of them will be

156 explained in more detail below.

157 **AtomType object**

158 The *AtomType* object is the most basic building block. This object bundles all the physical
159 constants (e.g. charge, atomic weight, scattering factors) for a single ion (e.g. Fe²⁺, Fe³⁺)
160 or for a molecule (e.g. H₂O and ethylene glycol) small enough to be considered having a
161 spherical electron cloud. When a new project is created, a default list of these *AtomType*
162 objects is loaded, using the atomic scattering factors as published by Waasmaier and
163 Kirfel (1995).

164 **Phase and Component objects**

165 *Phase* objects contain all the information needed to calculate a one-dimensional X-ray
166 diffraction pattern of a (mixed-layer) mineral. A *Phase* combines (i) a *Probability* object, (ii)
167 an object describing the coherent scattering domain size (*CSDS*), and (iii) one or more
168 *Component* objects which contain information about the structure of the different types of
169 layers in the *Phase*.

170 The *Probability* object describes how these layers are stacked by means of Markovian
171 statistics and the Reichweite concept (Drits and Tchoubar, 1990). Currently PyXRD has
172 implemented probability models for R values ranging from 0 to 3. For each combination of
173 Reichweite and number of components there are a number of independent parameters
174 required to calculate the remaining parameters, which describe the stacking order or
175 disorder. The values of these independent parameters can be based on another phase
176 with the same combination of Reichweite and number of components. For example, this
177 means it is possible to share the illite content in an illite/smectite mixed layer across its AD
178 and EG phase, but have different weight fractions (or junction probabilities) for the different
179 types of smectite in those phases. For a complete explanation on how these calculations

180 work and which parameters were chosen to be independent we refer to the manual.
181 The *CSDS* object describes what type of coherent scattering domain size distribution
182 should be used and contains the necessary parameter values to describe this distribution
183 (e.g. average CSDS). Two types of CSDS distributions are currently implemented: a
184 generic log-normal distribution and a log-normal distribution in which the distribution
185 constants published in Drits et al. (1997) are employed and the average CSDS is the only
186 remaining unknown variable. Each phase also has a σ^* factor which makes it possible to
187 correct for incomplete preferred orientation (Reynolds Jr., 1986; Dohrmann et al., 2009).
188 The *Component* object describes the size, structure, composition and (variation in) basal
189 spacing of a single layer type in that phase. A *Component* contains two lists that combine
190 an *AtomType* from the project with its (projected) coordinate along the c^* -axis (also known
191 as the z coordinate) and the number of projected ions of that type at that coordinate. The
192 first list involves atoms in the silicate lattice, while the other list describes the (variable)
193 interlayer space. With this approach, the silicate structure can be shared between different
194 phases (e.g. AD and EG states), while the interlayer contents may still be different.

195 **Specimen objects**

196 *Specimen* objects provide all the information regarding the experimental data (the actual
197 measurements, sample size, etc.) and the *Goniometer* set-up (radius, slit sizes, etc.). They
198 do not hold a direct reference to phases, but are linked with them through *Mixture* objects.

199 **Mixture objects**

200 *Mixture* objects are the starting point for the actual calculations as they link phases and
201 specimens together. In the user interface, a table can be created by adding just as many
202 rows as there are *Phases* and just as many columns as there are *Specimens*. In the
203 column headers, there are slots where the user can select the *Specimen*. Similarly, the

204 user can select the corresponding *Phase* in each cell of the table. This enables the user to
205 select different states of smectite for an AD and an EG *Specimen* (see figure 2 for a
206 screenshot of the GUI), while keeping unaffected *Phases*, (e.g. kaolinites, micas and
207 chlorites) unchanged.

208 Once a *Mixture* is created in this way, a number of parameters are available for automatic
209 refinement (e.g. weight fractions from the *Probability* object, the average CSDS, etc.). In a
210 refinement dialog, the user can select which parameters s/he would like to improve and
211 the minimum and maximum values between which the ideal value should lie. A number of
212 different refinement methods are also available - some of them more complex or
213 specialized than others. Yet, as a complete description of all methods is beyond the scope
214 of this article, only the algorithm used for the refinements will be explained in detail below.

215 **2.3 Numerical calculations**

216 The X-ray diffraction patterns are calculated using the matrix formalism, for which a very
217 good summary can be found in Drits and Tchoubar (1990). Later developments
218 incorporated can be found in Drits et al. (1997) and Plançon (2001). Since the complete
219 mathematical deduction followed for PyXRD is rather long, in itself does not contain new
220 developments, and is not the aim of this paper it is not included here. However, an
221 overview of the mathematical deductions and calculations, as they are implemented in the
222 'calculations' module, can be found in the online manual
223 (<http://users.ugent.be/~madumon/pyxrd/Manual.pdf>) or in the manual included in this
224 article's supplement.

225 To improve calculation speed, programs can make use of multi-threading, spreading the
226 load from the different threads evenly over the different cores in a multi-core CPU.
227 However, multi-threading is not very effective in Python because of the Global Interpreter
228 Lock (GIL). This lock can only be obtained by a single active thread, while the others have

229 to wait for it to be released again. So instead of multi-threading, PyXRD uses multi-
230 processing, which creates a new python interpreter for each process, circumventing the
231 GIL problem. The downside is that processes, unlike threads, do not share memory.
232 Therefore, each process needs to be given all the data required to run the calculation. This
233 is achieved by isolating the calculation functions from objects and by extracting the
234 required data from the objects described in the previous section. As a result, the data
235 exchanged between processes is reduced to a minimum.

236 This approach also makes it possible to run PyXRD refinements effectively on high-
237 performance computing (HPC) clusters. The experiments presented in this paper were run
238 on the HPC clusters of the Stevin Supercomputer Infrastructure at Ghent University. The
239 main reason to run these experiments on an HPC cluster was the large number of
240 replicates (50) involved in this work and the practical aspect of not having to dedicate a
241 separate PC. This does not mean refinements take too long on a regular PC; e.g. a
242 refinement with a dozen parameters finishes in less than 15 minutes on a 64-bit quad-core
243 3.10 GHz Intel® Core i5-2400 system. The setup on an HPC cluster is also more
244 cumbersome as it requires the user to get PyXRD to work on the cluster and submit a
245 working job script for his/her refinement from a command line. Running a refinement on a
246 local PC is much easier as the refinement algorithm (see below) and its parameters can be
247 selected and run from the GUI itself.

248 **2.4 Refinement algorithm**

249 PyXRD supports several refinement algorithms, but for more complex problems involving
250 several parameters, the genetic algorithms or evolutionary strategies are found to be most
251 reliable. PyXRD implements several evolutionary strategies, among which are a
252 Covariance Matrix Adaptation Evolutionary Strategy (Hansen and Ostermeier, 2001) and a
253 (multiple) Particle Swarm Optimization (Blackwell et al., 2008). While the Particle Swarm

254 Optimization is effective at searching the parameter space for minima, being able to
255 escape local minima easily, it can take a lot of function calls for it to converge. On the other
256 hand, the Covariance Matrix Adaptation Evolutionary Strategy is much more effective for
257 local searches, but does get stuck in local minima more easily. Therefore, PyXRD also
258 implements a Particle Swarm Covariance Matrix Adaptation Evolutionary Strategy
259 algorithm which extends the Covariance Matrix Adaptation Evolutionary Strategy with
260 collaborative concepts from a Particle Swarm Optimization (Muller et al., 2009), making it
261 the more robust choice. This Particle Swarm Covariance Matrix Adaptation Evolutionary
262 Strategy was also used for the experiments presented below.

263 **3. Results**

264 In the following sections PyXRD's output is compared with Sybilla's output. In the first
265 section, single phases are tested to check the implementation of the model. In the second
266 section a number of assemblages are tested to check if the obtained weight fractions are
267 correct. In the last section a comparison is made between single- versus multispecimen
268 refinements.

269 **3.1 Comparison between Sybilla and PyXRD results: calculated 00l** 270 **reflections for single discrete and mixed-layer phyllosilicates**

271 In total, 13 phases were tested. An overview of these phases with their most important
272 structural parameters are given in table 1. The original Sybilla projects, the produced
273 patterns and the PyXRD projects used can be found in this paper's supplement. All
274 patterns were calculated using a fixed σ^* value of 12, a sample length of 1.25 cm, a
275 goniometer radius of 17.3 cm, a divergence slit of 0.5° , Soller slits of 2.3° and an angular
276 range of 2° - 52° 2θ with 1000 steps (step size of 0.05° 2θ). The z^* coordinates of the atoms
277 were set to match with those in Sybilla, as were the scattering factors, the unit cell

278 dimension in the z direction, the octahedral iron content (for illite, chlorite and smectite
279 components), the interlayer water, ethylene glycol and cation contents (for smectite and
280 illite components) and the average coherent scattering domain size. The probability
281 parameters were entered as such that identical P and W matrices were obtained. For most
282 of the phases this meant identical parameters could be entered. Only for the R2
283 illite/smectite with two components 2 additional parameters were entered in comparison
284 with Sybilla, which has a more restricted probability model for this combination of
285 Reichweite and components. These parameters are the junction probabilities P_{21} (fixed at
286 1.0 in Sybilla) and P_{221} (fixed at 0.0 in Sybilla). A complete deduction on how the entered
287 probabilities and weight fractions are used to calculate the unknown weight and probability
288 fractions is present in the PyXRD manual. Sybilla uses scattering factors for the atoms in
289 the silicate lattice assuming 50% ionization, with the exception of Mg which is fully ionized
290 (D. McCarty, 2015). The scattering factors used in PyXRD for this study have been set to
291 match this.

292 The kaolinite, illite, talc and chlorite phases are composed of a single component. As such,
293 these are testing the basic aspects of the model such as the orientation factor σ^* , the
294 calculation of the coherent scattering domain size and the calculation of the atomic
295 scattering and structure factors. To test whether PyXRD can handle different sample states
296 correctly, an R0 two-component smectite in air-dried and glycolated state is modelled as
297 well. To further test the implementation of the matrix algorithm for mixed-layer phases, and
298 the related probability models, a number of illite/smectite phases were used. In total seven
299 phases were tested, four of which are two-component illite/smectite phases with
300 Reichweite values varying from 0 to 3 and three of which are three-component
301 illite/smectite phases with Reichweite values varying from 0 to 2. The different smectite
302 components have different hydration states, i.e. the first component always has 2 planes

303 of water (AD state) or 2 planes of ethylene glycol molecules (EG state) in its interlayer
304 space while the second component has only a single layer of water or ethylene glycol
305 molecules. For these illite/smectites two variants were calculated: one with a low CSDS
306 not at maximum possible degree of ordering (MPDO) and one with a higher CSDS at
307 MPDO.

308 Table 1 contains the Rp factor obtained for these test cases. A few of these patterns are
309 presented in figures 3 and 4. From them and from the Rp and Rwp factors, it is clear
310 PyXRD can produce patterns almost identical to those produced by Sybilla. The small
311 deviations can probably be explained by different physical constants (e.g. atomic
312 scattering factors), although it is impossible to know exactly.

313 **3.2 Comparison between Sybilla and PyXRD results: calculated 00l** 314 **reflections for mixtures of discrete and mixed-layer phyllosilicates**

315 To further validate the model, five patterns were produced in PyXRD for mixtures of
316 increasing complexity. These patterns were imported in Sybilla and modelled using the
317 same phases and the same parameters. This should allow to validate whether the weight
318 fractions in PyXRD can also be obtained by Sybilla. The entered and obtained weight
319 fractions and the corresponding Rp and Rwp factors are presented in table 2. Figure 5
320 shows the comparison between the calculated patterns for mixture 5 from Sybilla and
321 PyXRD. The used phases are largely identical to the phases used in the previous
322 validation, except for the addition of a few phases for which details are also given in table
323 2. The input files for PyXRD and Sybilla are included in this paper's supplement.

324 As can be observed, the weight fractions in PyXRD and Sybilla are reasonably close to
325 each other, with all of the deviations being smaller than 0.5 wt%. Such differences are not
326 to be considered significant for a real sample, but when using 'ideal' theoretical phases

327 they do indicate there are differences between Sybilla and PyXRD. In order to check if
328 some phases contribute more or less than others to the whole-pattern misfit, R_p and R_{wp}
329 factors are calculated for angular ranges corresponding to first-order reflections for the
330 phases in mixtures 1, 2 and 3 (table 3). This was not done for mixtures 4 and 5 due to the
331 presence of too many overlapping peaks, making statements about the contribution of
332 separate phases to the total misfit difficult. The R_p and R_{wp} factors obtained in this way
333 are all of the same order of magnitude. Therefore each phase must be contributing more
334 or less equally towards the whole-pattern misfit. The remaining differences between the
335 patterns can be explained by small differences in physical constants, while the remaining
336 differences in wt% can be explained by differences in unit cell dimensions.

337 **3.3 Multispecimen tests**

338 **3.3.1 Assemblage setup**

339 In total, four theoretical mineral assemblages were tested (table 4):

340 Assemblage 1 is a very simple test because of the absence of overlapping and similar
341 phases. Its main purpose was to see whether the program and, more importantly, the
342 selected refinement strategy, can produce a reliable result. The assemblage consists of
343 equal amounts of a discrete kaolinite, a discrete illite and an R0 illite/smectite with only
344 10% illite layers

345 Assemblage 2 is more complex, comprising six different phases: a discrete illite, a
346 discrete kaolinite, an R0 illite/smectite with 65% illite layers, an R0 kaolinite/smectite with
347 80% kaolinite layers, a smectite and a poorly-crystalline chlorite. The idea behind this
348 assemblage was to mimic phases encountered in some soils. The poorly-crystalline
349 chlorite component can be interpreted as a small amount of hydroxy-interlayered smectite
350 (or vermiculite) and is not to be considered a primary trioctahedral chlorite, while the

351 kaolinite/smectite represents a neoformed, defective kaolinite or smectite. This kind of
352 phase has been reported a number of times, usually in finer clay fractions ($\leq 0.2 \mu\text{m}$) of
353 certain soils (Hubert et al., 2009, 2012; Ryan and Huertas, 2009; Dumon et al., 2014). The
354 different phases are also present in different quantities, with the illite-bearing phases each
355 contributing 25.0 wt%, the smectite taking up 20.0 wt%, the kaolinite phases each
356 accounting for 12.5 wt% and the chlorite being a minor phase with only 5.0 wt%.

357 Assemblage 3 is composed of 30% discrete illite, 35% kaolinite, 20% high-charge
358 smectite (vermiculite-like) and 15% low-charge smectite. The main idea behind this test
359 assemblage was to see whether the presence of high-charge and low-charge phases
360 (which in this case produced similar patterns under AD and heated conditions, but different
361 patterns under EG conditions) has an influence on the refinement and the quantification in
362 the different set-ups.

363 Test patterns for assemblage 4 were calculated with 35% well-crystallized kaolinite (with
364 a high average CSDS), 15% poorly-crystallized kaolinite (with a low average CSDS) and
365 50% of an R0 illite/smectite with 98% of illite layers. However, these patterns were not
366 modelled with the same structural models. Instead of two different kaolinites, a single
367 kaolinite was added, and instead of an illite/smectite, a discrete illite was used. As such,
368 the influence of a simplified model input could be checked, which is a common error in
369 real-life uses (e.g. due to misinterpretation).

370 After the necessary phases and their parameters were set up, a calculated pattern was
371 generated from 2 to 50 $^{\circ}2\theta$ with a 0.02° step size, saved and re-imported as experimental
372 data. Random noise was also added to these patterns, using the following formula:

$$373 \quad I_n = I_o \cdot (1 + (X - 0.5) \cdot f_n)$$

374 where I_n is the intensity with noise, I_o the original intensity, X a random fraction between 0
375 and 1 and f_n the noise factor, which was set to 0.01. This results in a random deviation of

376 at most 0.5% above or below the original intensity. This is a high noise level when only
377 considering statistical counting noise, however, these noise levels can be obtained on iron-
378 rich samples when working with a Cu X-ray source due to iron fluorescence. Energy
379 dispersive detectors can eliminate most of this noise nowadays, but it can still be a
380 problem on older equipment, hence it is included here.

381 For assemblages 1 and 2, both the smooth and noisy patterns were used in separate
382 refinements to assess the influence of this treatment. For assemblages 3 and 4, only the
383 noisy patterns were used, because the previous two experiments showed little influence of
384 the noise on the final results (see below).

385 Since evolutionary refinement strategies have a stochastic component, each refinement
386 will be different, even if starting and boundary conditions are identical. Nonetheless, the
387 starting point may also have an influence on the final result. To average out these
388 differences and to check if the final output is reproducible, 50 random starting points were
389 sampled so that a normal distribution over the parameter space was obtained. For each of
390 these points a refinement was started. At the end of these refinements, average parameter
391 values and their standard deviations were calculated for these 50 iterations. Additionally,
392 the model kept track of the best solution found at each generation in each iteration,
393 allowing us to create parameter evolution plots.

394

395 **3.3.2 Assemblage 1**

396 An overview of the obtained average parameter values and standard deviations for
397 assemblage 1 can be found in tables 5 and 6. Parameter evolution plots for two selected
398 parameters (the average CSDS and the fraction of illite layers in the illite/smectite) are also
399 shown in figure 6. Most parameters are determined accurately and with very high
400 precision. The difference between noisy patterns and smooth patterns is marginal, and no

401 difference can be observed between the runs where multiple specimens are combined and
402 those where only a single specimen was used for refinement. As a result of this, the
403 obtained weight fractions for the three phases are also very accurate. The obtained level
404 of accuracy is not a realistic level for natural samples, but stems from the simplicity of this
405 set-up. For the runs using the noisy patterns, a very small (and systematic) deviation in the
406 obtained weight fractions can be observed. This is probably the result of the added noise,
407 since the deviation is not present for runs using the smooth patterns.

408

409 **3.3.3 Assemblage 2**

410 An overview of the obtained average parameter values and standard deviations for
411 assemblage 2 can be found in tables 7 and 8. As was the case in the previous
412 assemblage, no significant difference can be observed between runs that use smooth
413 patterns and those that use noisy ones. Both types produced similar parameter accuracies
414 and precisions. Overall, the results are less accurate and precise compared to
415 assemblage 1, but still very good. Most notably, the weight fractions of the smectite layer
416 types in the kaolinite/smectite show a much larger imprecision. This is also the case in the
417 parameter evolution plots (figure 7) for these fractions. An explanation can be found in the
418 sensitivity of these parameters: since the kaolinite fraction in this mixed-layer is relatively
419 high (80%), the relative amounts of the different types of smectite layers do not have such
420 a large influence on the calculated pattern. Some differences are also noticeable between
421 runs that combine multiple specimens and those where only heated patterns were used.
422 For the latter, the imprecision on the weight fractions for the illite, illite/smectite and
423 smectite phases is significantly larger compared to the other runs. This is to be expected,
424 as heating collapses swelling layers, causing significant peak overlap with the illite peaks.
425 Despite this overlap, it was still possible to obtain accurate and precise averages for the

426 other parameters, comparable to the other runs.

427 **3.3.4 Assemblage 3**

428 An overview of the obtained average parameter values and standard deviations for
429 assemblage 3 can be found in table 9. With this assemblage, the combined set-up and the
430 set-up using only the EG pattern both resulted in the same performance, giving accurate
431 and precise parameter values. The set-up with AD or heated patterns, on the other hand,
432 led to inaccurate and imprecise results, especially when the weight fractions are taken into
433 account. Finally, it can also be observed that the weight fractions and parameter values of
434 phases that were unaffected by the treatments (i.e. kaolinite and illite) are more accurate
435 and precise in these set-ups. It is mainly for the overlapping phases (i.e. smectites) that
436 the errors occur.

437 Figure 8 shows the parameter plots for the multispecimen set-up and the AD set-up for a
438 few selected parameters. This figure illustrates the divergent nature of some parameters in
439 the AD set-up very well, while it is clear that the combined set-up does not suffer from this
440 as it has access to the EG pattern as well.

441 The outcome of this experiment is in line with our expectations, as only the EG pattern
442 contains enough information to distinguish these two smectites from each other. When the
443 EG pattern is absent, the results become divergent, resulting in the high imprecision
444 observed for the AD and heated pattern set-ups.

445 **3.3.5 Assemblage 4**

446 An overview of the obtained average parameter values and standard deviations for
447 assemblage 4 can be found in table 10. In this set-up, we intentionally misidentified a
448 mixed-layer illite/smectite as an illite and overlooked the presence of two populations of
449 kaolinite instead of one. Nevertheless the flawed structural model is able to give us decent

450 parameter accuracies. These kinds of 'mistakes' are quite common in the real-life use of
451 this kind of program, and apparently do not matter too much either, as long as they are
452 related to natural inhomogeneities. In contrast, a model based on a completely wrong
453 interpretation will never yield any good output, and will result in a very obvious mismatch
454 between the calculated and observed patterns. Even in this assemblage, the (residual)
455 XRD patterns (figure 9) show a clear mismatch for these phases. An observant user
456 should notice this and as such be able to identify wrong and/or missing phases.

457 **3.3.6 Summary**

458 For all four assemblages, PyXRD has been able to reproduce the input parameters or at
459 least approximate them with the multispecimen approach. The only complications occur
460 when single patterns are used which do not contain enough information on their own (in
461 most cases heated patterns).

462 The results for these theoretical assemblages seem to suggest that the multi-specimen
463 approach does not add a lot of constraints to the mathematical model. Instead, it appears
464 far more important to correctly identify the phases using multiple specimens than to use
465 these for the parameter refinement. As a result, once the phases are correctly identified, a
466 good quantification can often be obtained with only a single pattern if all phases can be
467 sufficiently discerned from one another in that state. For most natural samples, this could
468 imply that it is sufficient to model the EG and/or the AD pattern. Indeed, many papers
469 presenting modelled X-ray diffraction patterns of phyllosilicates only use the AD and/or EG
470 patterns (Plançon and Roux, 2010; Hubert et al., 2012; Ufer et al., 2012a; Dumon et al.,
471 2014). However, it is important to realize that these results from theoretical experiments
472 cannot be extrapolated automatically to all real-life modelling experiments.

473 In this context, one needs to understand how realistic it is to share some of the parameters
474 between the different specimens during the refinement. Some of them are rather difficult or

475 impossible to control from measurement to measurement. For example, the number of
476 water or ethylene glycol planes intercalated into smectite bearing phases is not only
477 dependent on layer charge and the saturating cation, but also on the ambient conditions
478 (i.e. temperature and relative humidity) (Tamura et al., 2000). Because of this, a lot of the
479 parameters cannot and should not be shared, and the advantage of having added more
480 observations is partially lost.

481 **5. Conclusion**

482 In this paper we have presented PyXRD, a new, free and open-source program to perform
483 a (semi-)quantitative analysis of disordered layered minerals using multispecimen X-ray
484 diffraction profile fitting. It is the authors' sincere hope that others will pick up on the
485 program and improve it. The novelty of this program lies specifically in the *ab initio*
486 incorporation of the multispecimen method, making it possible to share phases and (a
487 selection of) their parameters across multiple specimens. This allows to model several
488 specimens side-by-side, and is an important step forward. In theory, this could also help in
489 further constraining the mathematical model and thus improving the automatic parameter
490 refinement results (Sakharov et al., 1999a; Meunier, 2005; Lanson, 2011). However,
491 results from theoretical experiments indicate that a multispecimen refinement setup is not
492 always required to obtain good parameter estimates. Finally, it remains of paramount
493 importance to use the multispecimen method to obtain a correct identification, as without it
494 no meaningful quantification can ever be obtained. We can conclude that PyXRD has
495 proven to be very useful when X-ray diffraction patterns for complex mineral assemblages
496 containing (mixed-layer) phyllosilicates are modelled with a multispecimen approach.

497 **6. Code availability**

498 The source code for PyXRD can be found online at <https://github.com/mathijs->

499 [dumon/PyXRD](#), together with installation instructions and a manual with detailed
500 information regarding the calculations and a step-by-step example on how to use the user
501 interface.

502 **7. Acknowledgements**

503 This research was funded by the project G028714N of the Fund for Scientific Research
504 (Flanders). The computational resources (Stevin Supercomputer Infrastructure) and
505 services used in this work were provided by the VSC (Flemish Supercomputer Center),
506 funded by Ghent University, the Hercules Foundation and the Flemish Government
507 (Department EWI), for which we are very grateful.

508 **8. References**

- 509 Agbenin, J.O., and Tiessen, H., 1995. Soil properties and their variations on two
510 contiguous hill slopes in Northeast Brazil. *Catena* 24, 147–161.
- 511 Aplin, A.C., Matenaar, I.F., McCarty, D.K., and van der Pluijm, B.A., 2006. Influence of
512 mechanical compaction and clay mineral diagenesis on the microfabric and pore-
513 scale properties of deep-water Gulf of Mexico mudstones. *Clays Clay Miner* 54, 500–
514 514.
- 515 Blackwell, T., Branke, J., and Li, X., 2008. Particle Swarms for Dynamic Optimization
516 Problems. p. 193–217. *In* Blum, C., Merkle, D. (eds.), *Swarm Intelligence*. Natural
517 Computing Series. Springer Berlin Heidelberg.
- 518 Caner, L., Hubert, F., Moni, C., and Chenu, C., 2010. Impact of clay mineralogy on
519 stabilisation of organic matter in the clay fraction of a Neo-Luvisol and a Cambisol.
520 p. 73–76. *In* 19th World Congress of Soil Science: Soil Solutions for a Changing
521 World. Brisbane, Australia.
- 522 McCarty, D., (2015, October 1). Personal communication - Sybilla, Computer
523 software version 2.2.2 © Chevron Technology Company, a division of Chevron,
524 U.S.A. Inc., San Ramon, CA.
- 525 Cornelis, J.-T., Weis, D., Lavkulich, L., Vermeire, M.-L., Delvaux, B., and Barling, J., 2014.
526 Silicon isotopes record dissolution and re-precipitation of pedogenic clay minerals in
527 a podzolic soil chronosequence. *Geoderma* 235–236, 19–29.
- 528 Dazas, B., Lanson, B., Delville, A., Robert, J.-L., Komarneni, S., Michot, L.J., and Ferrage,
529 E., 2015, Influence of Tetrahedral Layer Charge on the Organization of Interlayer
530 Water and Ions in Synthetic Na-Saturated Smectites: *The Journal of Physical*
531 *Chemistry C*, v. 119, no. 8, p. 4158–4172, doi: 10.1021/jp5123322.
- 532 Dohrmann, R., Rüping, K.B., Kleber, M., Ufer, K., and Jahn, R., 2009. Variation of

533 preferred orientation in oriented clay mounts as a result of sample preparation and
534 composition. *Clays Clay Miner* 57, 686–694.

535 Drits, V.A., 1997. Mixed-layer minerals. p. 153–190. *In* Merlino, S. (ed.), *Modular Aspects*
536 *of Minerals*. EMU Notes in Mineralogy. Eötvös University Press, Budapest.

537 Drits, V., Środoń, J., and Eberl, D.D., 1997. XRD Measurement of mean crystallite
538 thickness of illite and illite/smectite: reappraisal of the Kubler Index and the Scherrer
539 Equation. *Clays Clay Miner* 45, 461–475.

540 Drits, V.A., and Sakharov, B.A., 1976. X-ray structure analysis of interstratified minerals.
541 Nauka, Moscow, 225 pp (in Russian).

542 Drits, V.A., and Tchoubar, C., 1990. X-Ray Diffraction by Disordered Lamellar Structures:
543 Theory and Applications to Microdivided Silicates and Carbons. Springer-Verlag,
544 Berlin, Germany.

545 Dumon, M., Tolossa, A.R., Capon, B., Detavernier, C., and Van Ranst, E., 2014.
546 Quantitative clay mineralogy of a Vertic Planosol in southwestern Ethiopia: Impact on
547 soil formation hypotheses. *Geoderma* 214-215, 184–196.

548 Ergun, S. (1970). X-ray scattering by very defective lattices. *Phys. Rev. B*, 131, 3371-
549 3380.

550 Ferrage, E., Lanson, B., Sakharov, B.A., Geoffroy, N., Jacquot, E., and Drits, V.A., 2007.
551 Investigation of dioctahedral smectite hydration properties by modeling of X-ray
552 diffraction profiles: Influence of layer charge and charge location. *American*
553 *Mineralogist* 92, 1731–1743.

554 Ferrage, E., Lanson, B., Malikova, N., Plancon, A., Sakharov, B.A., and Drits, V.A., 2005a.
555 New Insights on the Distribution of Interlayer Water in Bi-Hydrated Smectite from X-
556 ray Diffraction Profile Modeling of 00l Reflections. *Chem Mater* 17, 3499–3512.

557 Ferrage, E., Lanson, B., Sakharov, B.A., and Drits, V.A., 2005b. Investigation of smectite

558 hydration properties by modeling experimental X-ray diffraction patterns: Part I.
559 Montmorillonite hydration properties. *American Mineralogist* 90, 1358–1374.

560 Fortin, F.-A., De Rainville, F.-M., Gardner, M.-A., Parizeau, M., and Gagné, C., 2012.
561 DEAP: Evolutionary Algorithms Made Easy. *JMLR* 13, 2171–2175.

562 Hansen, N., and Ostermeier, A., 2001. Completely Derandomized Self-Adaptation in
563 Evolution Strategies. *Evol. Comput.* 9, 159–195.

564 Hubert, F., Caner, L., Meunier, A., and Ferrage, E., 2012. Unraveling complex <math><2\mu\text{m}</math> clay
565 mineralogy from soils using X-ray diffraction profile modeling on particle-size sub-
566 fractions: Implications for soil pedogenesis and reactivity. *Am Mineral* 97, 384–398.

567 Hubert, F., Caner, L., Meunier, A., and Lanson, B., 2009. Advances in characterization of
568 soil clay mineralogy using X-ray diffraction: from decomposition to profile fitting.
569 *European Journal of Soil Science* 60, 1093–1105.

570 Hunter, J.D., 2007. Matplotlib: A 2D Graphics Environment. *Computing in Science &*
571 *Engineering* 9, 90–95.

572 Jones, E., Oliphant, T., and Peterson, P., 2001. SciPy: Open Source Scientific Tools for
573 Python.

574 Kakinoki, J. and Komura, Y. (1965) Diffraction by a one-dimensionally disordered crystal. I:
575 The intensity equation. *Acta Cryst.*, 19, 137-147.

576 Lado, M., and Ben-Hur, M., 2004. Soil mineralogy effects on seal formation, runoff and soil
577 loss. *Appl. Clay Sci.* 24, 209–224.

578 Lanson, B., 2011. Modelling of X-ray diffraction profiles: Investigation of defective lamellar
579 structure crystal chemistry. p. 151–202. *In* Brigatti, M.F., Mottana, A. (eds.), *Layered*
580 *mineral structures and their Application in Advanced Technologies*. EMU Notes in
581 *Mineralogy*.

582 Meunier, A., 2005. *Clays*. Springer, Berlin, Germany.

583 Meunier, A., 2007. Soil Hydroxy-Interlayerd minerals: a re-interpretation of their
584 crystallochemical properties. *Clays Clay Miner* 55, 380–388.

585 Michot, L.J., Bihannic, I., Pelletier, M., Rinnert, E., and Robert, J.-L., 2005, Hydration and
586 swelling of synthetic Na-saponites: Influence of layer charge: *American Mineralogist*,
587 v. 90, no. 1, p. 166–172.

588 Muller, C.L., Baumgartner, B., and Sbalzarini, I., 2009. Particle Swarm CMA Evolution
589 Strategy for the optimization of multi-funnel landscapes. p. 2685–2692. *In* IEEE
590 Congress on Evolutionary Computation, 2009. CEC '09.

591 Pai, C.W., Wang, M.K., King, H.B., Chiu, C.Y., and Hwong, J.-L., 2004. Hydroxy-
592 interlayered minerals of forest soils in A-Li Mountain, Taiwan. *Geoderma* 123, 245–
593 255.

594 Pevear, D.R., and Schuette, J.F., 1993. Inverting the NEWMOD[®] X-ray Diffraction Forward
595 Model for Clay Minerals Using Genetic Algorithms. p. 19–42. *In* Computer
596 Applications to X-ray Powder Diffraction Analysis of Clay Minerals Vol. 5. Clay
597 Minerals Society, Boulder, Colorado.

598 Plançon A., 1981. Diffraction by layer structures containing different kinds of layers and
599 stacking faults. *Journal of Applied Crystallography*, 14, 300-304.

600 Plançon, A., 2001. Order-disorder in clay mineral structures. *Clay Miner* 36, 1–14.

601 Plançon, A., and Drits, V.A., 2000. Phase analysis of clays using an expert system and
602 calculation programs for x-ray diffraction by two- and three-component mixed layer
603 minerals. *Clays Clay Miner* 48, 57–62.

604 Plançon, A., and Roux, J., 2010. Software for the assisted determination of the structural
605 parameters of mixed-layer phyllosilicates. *European Journal of Mineralogy* 22, 733–
606 740.

607 Reynolds, R.C., 1967. Interstratified clay systems: calculation of total one-dimensional

608 diffraction functions. *American Mineralogist*, 52, 661–672.

609 Reynolds Jr, R.C., 1985. NEWMOD: a computer program for the calculation of one-
610 dimensional diffraction patterns of mixed-layer clays, R.C. Reynolds, Hanover, NH,
611 USA

612 Reynolds Jr, R.C., 1986. The Lorentz-Polarisation factor and preferred orientation in
613 oriented clay aggregates. *Clays Clay Miner* 34, 359–367.

614 Reynolds Jr, R.C., and Reynolds III, R.C., 1996. NEWMOD-for-Windows. The Calculation
615 of One-Dimensional X-ray Diffraction Patterns of Mixed Layered Clay
616 Minerals. Computer program, RC Reynolds, Hanover, NH, USA.

617 Righi, D., Terribile, F., and Petit, S., 1999. Pedogenic formation of kaolinite-smectite mixed
618 layers in a soil toposequence developed from basaltic parent material in Sardinia
619 (Italy). *Clays Clay Miner* 47, 505–514.

620 Ryan, P.C., and Huertas, F.J., 2009. The temporal evolution of pedogenic Fe–smectite to
621 Fe–kaolin via interstratified kaolin–smectite in a moist tropical soil chronosequence.
622 *Geoderma* 151, 1–15.

623 Sakharov, B. A. and Drits, V. A., 1973. Mixed-layer kaolinite-montmorillonite: a comparison
624 of observed and calculated diffraction patterns. *Clays Clay Miner* 21, 15-17.

625 Sakharov, B.A., Lindgreen, H., Salyn, A., and Drits, V.A., 1999a. Determination of illite-
626 smectite structures using multispecimen x-ray diffraction profile fitting. *Clays Clay*
627 *Miner* 47, 555–566.

628 Sakharov, B.A., Lindgreen, H., Salyn, A.L., and Drits, V.A., 1999b. Mixed-layer kaolinite-
629 illite-vermiculite in North Sea shales. *Clay Miner* 34, 333–344.

630 Środoń, J., 2006. Identification and Quantitative Analysis of Clay Minerals. p. 765–787. *In*
631 *Handbook of Clay Science. Developments in Clay Science.* Elsevier, USA.

632 Treacy, M. M. J., Newsam, J. M. & Deem, M. W. (1991). A General Recursion Method for

633 Calculating Diffracted Intensities from Crystals Containing Planar Faults. P Roy Soc
634 Lond A, 433, 499–520.

635 Tamura, K., Yamada, H., and Nakazawa, H., 2000. Stepwise Hydration of High-Quality
636 Synthetic Smectite with Various Cations. *Clays Clay Miner* 48, 400–404.

637 Toby, B.H., 2006. R factors in Rietveld analysis: How good is good enough? *Powder Diffr*
638 21, 67-70.

639 Ufer, K., Kleeberg, R., Bergmann, J., and Dohrmann, R., 2012a. Rietveld refinement of
640 disordered illite-smectite mixed-layer structures by a recursive algorithm. I: One-
641 dimensional patterns. *Clays Clay Miner* 60, 507–534.

642 Ufer, K., Kleeberg, R., Bergmann, J., and Dohrmann, R., 2012b. Rietveld refinement of
643 disordered illite-smectite mixed-layer structures by a recursive algorithm. II: Powder-
644 pattern refinement and quantitative phase analysis. *Clays Clay Miner* 60, 535–552.

645 Velde, B.B., and Meunier, A., 2008. *The Origin of Clay Minerals in Soils and Weathered*
646 *Rocks*. Springer-Verlag, Berlin, Germany.

647 Vernik, L., and Liu, X., 1997. Velocity anisotropy in shales: A petrophysical study:
648 *Geophysics*, 62, 521–532.

649 Viennet, J.C. Hubert, F., Ferrage, E., Tertre, E., Legout, A. and Turpault, M.P., 2015.
650 Investigation of clay mineralogy in a temperate acidic soil of a forest using X-ray
651 diffraction profile modelling: Beyond the HIS and HIV description. *Geoderma* 241–
652 242, 75–86.

653 Waasmaier, D., and Kirfel, A., 1995. New analytical scattering-factor functions for free
654 atoms and ions. *Acta Crystallographica Section A Foundations of Crystallography* 51,
655 416–431.

656 Wen, B.P., and Aydin, A., 2003. Microstructural study of a natural slip zone: quantification
657 and deformation history. *Engineering Geology*, 68, 289–317.

658 Van der Walt, S., Colbert, S.C., and Varoquaux, G., 2011. The NumPy Array: A Structure
659 for Efficient Numerical Computation. *Computing in Science & Engineering* 13, 22–30.

660 Yuan, H., and Bish, D.L., 2010. NEWMOD+, a new version of the NEWMOD program for
661 interpreting x-ray powder diffraction patterns from interstratified clay minerals. *Clays
662 Clay Miner* 58, 318–326.

Table 1: Overview of the discrete phases used to compare the output from PyXRD with the output of Sybilla (R is Reichweite, G is the number of components, \bar{N} is the average CSDS, AD is air-dry, EG is ethylene-glycol, relevant probability (P) and weight (W) factors are given, Rp and Rwp are the unweighted and weighted residual errors of the patterns respectively).

	Phase	R	G	State	\bar{N}	P and W factors			Rp	Rwp
1	Kaolinite	-	1	-	20	-			0.7	0.9
2	Illite	-	1	-	20	-			0.9	1.3
3	Talc	-	1	-	20	-			0.8	1.0
4	Chlorite	-	1	-	20	-			0.8	1.0
5	Illite/Smectite	0	2	AD	4	$W_1 = 0.5$			1.0	1.6
6	Illite/Smectite	1	2	AD	4	$W_1 = 0.6$ $P_{22} = 0.5$			1.0	1.6
6b	Illite/Smectite	1	2	AD	15	$W_1 = 0.6$ $P_{22} = 0.0$			0.7	1.5
7	Illite/Smectite	2	2	AD	4	$W_1 = 0.6$ $P_{21} = 1.0$	$P_{112} = 0.5$ $P_{221} = 0.0$		1.4	2.1
7b	Illite/Smectite	2	2	AD	15	$W_1 = 0.6$ $P_{21} = 1.0$	$P_{112} = 1.0$ $P_{221} = 0.0$		0.7	1.5
8	Illite/Smectite	3	2	AD	4	$W_1 = 0.9$ $P_{2112} = 0.5$	$P_{22}=0$ $P_{212}=0$		1.9	2.3
8b	Illite/Smectite	3	2	AD	15	$W_1 = 0.9$ $P_{2112} = 0.0$	$P_{22}=0$ $P_{212}=0$		0.5	1.0
9	Illite/Smectite	0	3	AD	4	$W_1 = 0.33$ $W_2 / (W_2+W_3) = 0.5$			1.1	1.7
10	Illite/Smectite	1	3	AD	4	$W_1 = 0.5$ $W_2 / (W_2+W_3) = 0.8$	$P_{11} = 0.85$ $(W_{22}+W_{23}) / (W_{22}+W_{23}+W_{32}+W_{33}) = 0.85$	$W_{22} / (W_{22}+W_{23}) = 0.8$ $W_{32} / (W_{32}+W_{33}) = 0.7$	1.1	1.7
10b	Illite/Smectite	1	3	AD	15	$W_1 = 0.5$ $W_2 / (W_2+W_3) = 0.8$	$P_{11} = 0.0$ $(W_{22}+W_{23}) / (W_{22}+W_{23}+W_{32}+W_{33}) = 0.85$	$W_{22} / (W_{22}+W_{23}) = 0.8$ $W_{32} / (W_{32}+W_{33}) = 0.7$	1.0	1.7
11	Illite/Smectite	2	3	AD	4	$W_1 = 0.8$ $W_2 / (W_2+W_3) = 0.5$	$P_{x1x} = 0.5$ $(W_{212}+W_{213}) / (W_{212}+W_{213}+W_{312}+W_{313}) = 0.5$	$W_{212} / (W_{212}+W_{213}) = 0.5$ $W_{312} / (W_{312}+W_{313}) = 0.5$	1.7	2.2
11b	Illite/Smectite	2	3	AD	15	$W_1 = 0.8$ $W_2 / (W_2+W_3) = 0.5$	$P_{x1x} = 0.0$ $(W_{212}+W_{213}) / (W_{212}+W_{213}+W_{312}+W_{313}) = 0.5$	$W_{212} / (W_{212}+W_{213}) = 0.5$ $W_{312} / (W_{312}+W_{313}) = 0.5$	0.5	1.0
12	Smectite	0	2	AD	4	$W_1 = 0.7$			1.3	1.7
13	Smectite	0	2	EG	4	$W_1 = 0.7$			1.0	1.2

Table 2: Overview of the test mixtures used to compare the weight fraction output from PyXRD with the output of Sybilla, with details for the different phases (R is Reichweite, \bar{N} is the average CSDS, d_{001} is the basal spacing, relevant probability (P) and weight (W) factors are given).

Mixture	Rp	Rwp	Phases	PyXRD wt%	Sybilla wt%	Phase characteristics
1	0.8	1.0	Kaolinite	70.0	69.9	As in table 1
			Illite	30.0	30.1	As in table 1
2	1.1	1.5	Kaolinite	20.0	20.0	As in table 1
			Illite	30.0	30.1	As in table 1
			IS R0	10.0	9.5	As in table 1
			SSS R0	40.0	40.5	$\bar{N} = 4$; $W_1=0.8$; $W_2/(W_2+W_3)=0.8$
3	1.0	1.4	Kaolinite	10.0	10.0	As in table 1
			Illite	25.0	25.1	As in table 1
			Chlorite	20.0	20.1	As in table 1
			IS R0	15.0	14.7	As in table 1
			CS R1	10.0	10.1	$\bar{N} = 10$; $W_1=0.5$; $P_{11} = 0.1$
			SSS R0	20.0	20.0	$\bar{N} = 4$; $W_1=0.8$; $W_2/(W_2+W_3)=0.8$
4	1.3	1.8	ISS R0	15.0	15.2	As in table 1
			CSS R0	5.0	5.0	$\bar{N} = 5$; $W_1=0.4$; $W_2/(W_2+W_3)=0.9$
			Chlorite	5.0	5.0	As in table 1
			Illite	15.0	14.9	As in table 1
			Kaolinite 1	15.0	14.9	As in table 1
			Kaolinite 2	25.0	25.0	$\bar{N} = 6$; $d_{001} = 0.718$ nm
			IS R1	10.0	10.0	As in table 1
			CS R1	10.0	10.1	$\bar{N} = 10$; $W_1=0.5$; $P_{11} = 0.1$
5	1.7	2.4	ISS R0	10.0	10.0	As in table 1
			CSS R0	10.0	10.0	$\bar{N} = 5$; $W_1=0.4$; $W_2/(W_2+W_3)=0.9$
			Chlorite	10.0	10.0	As in table 1
			Illite	10.0	9.9	As in table 1
			Kaolinite 1	10.0	10.0	As in table 1
			Kaolinite 2	10.0	10.0	$\bar{N} = 6$; $d_{001} = 0.718$ nm
			IS R1	10.0	10.1	As in table 1
			CS R1	10.0	9.9	$\bar{N} = 10$; $W_1=0.5$; $P_{11} = 0.1$
			SS R0	10.0	9.9	$\bar{N} = 4$; $W_1=0.7$
			KSS R0	10.0	10.0	$\bar{N} = 7$; $W_1=0.6$; $W_2/(W_2+W_3)=0.8$

Table 3: Calculated Rp and Rwp values for selected intervals of mixtures 1, 2 and 3 calculated in PyXRD and Sybilla. (Rp and Rwp are the unweighted and weighted residual errors of the selected intervals respectively)

Angular range (°2θ)	Dominant phase(s)	Approximate d-spacing	Rp (%)	Rwp (%)
Mixture 1				
8.2-9.2	Illite	~ 1.0 nm	1.1	1.1
11.25-13.25	Kaolinite	~ 0.72 nm	0.6	0.9
Mixture 2				
4.5-7.0	IS R0 & SSS R0	~ 1.5 nm	0.9	1.1
8.2-9.2	Illite	~ 1.0 nm	0.5	0.6
11.25-13.25	Kaolinite	~ 0.72 nm	0.7	1.0
Mixture 3				
2.5-4.0	CS R1	~ 2.9 nm	0.8	0.8
4.5-7.0	IS R0, SSS R0 & CS R1	~ 1.5 nm	1.1	1.3
8.2-9.2	Illite	~ 1.0 nm	0.5	0.6
11.25-13.25	Kaolinite	~ 0.72 nm	0.5	0.7

Table 4: Overview of the different test assemblages for the comparison between multispecimen and single pattern refinements and the type of refined patterns.

	Assemblage	Smooth pattern?	Noisy pattern?
1	33.3% Kaolinite 33.3% Illite 33.3% Illite/Smectite (10/90) R0	yes	yes
2	25.0% Illite 25.0% Illite/Smectite (65/35) R0 20.0% Smectite 12.5% Kaolinite 12.5% Kaolinite/Smectite (80/20) R0 5.0% Chlorite	yes	yes
3	35.0% Kaolinite 30.0% Illite 15.0% High-charge smectite 20.0% Low-charge smectite	no	yes
4	35.0% Kaolinite (CSDS = 20) 15.0% Kaolinite (CSDS = 6) 50.0% Illite/Smectite (98/2) R0	no	yes

Table 5: Overview of the means and standard deviations for weight fractions and refined parameters for assemblage 1 using smooth patterns.

Assemblage #1 - smooth patterns			Range		Multiple specimens (n=50)	Only AD (n=50)	Only EG (n=50)	Only 350 heated (n=50)
Phase	Property name	True value	Min.	Max.	Obtained value $\mu \pm \sigma$	Obtained value $\mu \pm \sigma$	Obtained value $\mu \pm \sigma$	Obtained value $\mu \pm \sigma$
Kaolinite	wt%	33.3	–	–	33.3 ± 0.00	33.3 ± 0.00	33.3 ± 0.00	33.3 ± 0.00
	T	10.0	8.0	20.0	10.0 ± 0.00	10.0 ± 0.00	10.0 ± 0.00	10.0 ± 0.00
Illite	wt%	33.3	–	–	33.3 ± 0.00	33.3 ± 0.00	33.3 ± 0.00	33.3 ± 0.00
	T	10.0	8.0	20.0	10.0 ± 0.00	10.0 ± 0.00	10.0 ± 0.00	10.0 ± 0.00
Illite/Smectite R0	wt%	33.3	–	–	33.3 ± 0.00	33.3 ± 0.00	33.3 ± 0.00	33.3 ± 0.00
	T	5.0	3.0	10.0	5.0 ± 0.00	5.0 ± 0.00	5.0 ± 0.00	5.0 ± 0.00
	Illite content	0.1	0.0	1.0	0.10 ± 0.00	0.10 ± 0.00	0.10 ± 0.00	0.10 ± 0.00
	2wat / (2wat + 1wat)	0.5	0.0	1.0	0.50 ± 0.00	0.50 ± 0.00	–	–
	2 alv / (2alv + 1alv)	0.5	0.0	1.0	0.50 ± 0.00	–	0.50 ± 0.00	–
	0 alv / (0alv + 1alv)	1.0	0.0	1.0	1.00 ± 0.00	–	–	1.00 ± 0.00

Table 7: Overview of the means and standard deviations of weight fractions and refined parameters for assemblage 2 using smooth patterns.

<i>Assemblage #2 – Smooth patterns</i>					Multiple specimens (n=50)	Only AD (n=50)	Only EG (n=50)	Only 350°C (n=50)
Phase	Property name	True value	Range		Obtained value $\mu \pm \sigma$	Obtained value $\mu \pm \sigma$	Obtained value $\mu \pm \sigma$	Obtained value $\mu \pm \sigma$
			Min.	Max.				
Illite	wt%	25.0	–	–	25.0 ± 0.1	25.0 ± 0.1	25.0 ± 0.0	25.4 ± 0.71
	T	13.0	10.0	30.0	13.0 ± 0.1	13.0 ± 0.0	13.0 ± 0.0	12.9 ± 0.2
Illite/Smectite R0	wt%	25.0	–	–	24.9 ± 0.2	25.0 ± 0.1	25.0 ± 0.0	24.8 ± 0.3
	T	5.0	3.0	10.0	5.1 ± 0.1	5.0 ± 0.0	5.0 ± 0.0	5.0 ± 0.1
	Illite content	0.65	0.5	1.0	0.65 ± 0.00	0.65 ± 0.00	0.65 ± 0.00	0.64 ± 0.03
	2wat / (2wat + 1wat)	0.7	0.0	1.0	0.70 ± 0.01	0.70 ± 0.00	–	–
	2 alv / (2alv + 1alv)	0.7	0.0	1.0	0.71 ± 0.02	–	0.70 ± 0.00	–
	0 alv / (0alv + 1alv)	1.0	0.8	1.0	0.96 ± 0.03	–	–	0.99 ± 0.01
Kaolinite	wt%	12.5	–	–	12.5 ± 0.0	12.5 ± 0.0	12.5 ± 0.0	12.5 ± 0.0
	T	20.0	10.0	30.0	20.1 ± 0.1	20.0 ± 0.0	20.0 ± 0.0	20.1 ± 0.1
Kaolinite/Smectite R0	wt%	12.5	–	–	12.7 ± 0.2	12.5 ± 0.1	12.5 ± 0.0	12.9 ± 0.2
	T	3.0	3.0	10.0	3.0 ± 0.0	3.0 ± 0.0	3.0 ± 0.0	3.0 ± 0.0
	Kaolinite content	0.80	0.7	1.0	0.80 ± 0.01	0.80 ± 0.00	0.80 ± 0.00	0.79 ± 0.00
	2wat / (2wat + 1wat)	0.25	0.0	0.6	0.26 ± 0.11	0.25 ± 0.02	–	–
	2 alv / (2alv + 1alv)	0.50	0.0	0.6	0.44 ± 0.10	–	0.50 ± 0.01	–
	0 alv / (0alv + 1alv)	1.00	0.8	1.0	0.93 ± 0.05	–	–	0.93 ± 0.04
Smectite	wt%	20.0	–	–	19.9 ± 0.1	20.0 ± 0.1	20.0 ± 0.0	19.6 ± 0.7
	T	3.0	3.0	10.0	3.0 ± 0.0	3.0 ± 0.0	3.0 ± 0.0	3.0 ± 0.0
	2wat / (2wat + 1wat)	0.60	0.5	1.0	0.60 ± 0.00	0.60 ± 0.00	–	–
	2 alv / (2alv + 1alv)	0.90	0.5	1.0	0.90 ± 0.00	–	0.90 ± 0.00	–
	0 alv / (0alv + 1alv)	0.90	0.8	1.0	0.92 ± 0.01	–	–	0.90 ± 0.01
Chlorite	wt%	5.0	–	–	5.0 ± 0.0	5.0 ± 0.1	5.0 ± 0.0	5.0 ± 0.0
	T	5.0	3	10	5.0 ± 0.0	5.0 ± 0.0	5.0 ± 0.0	5.0 ± 0.0
	$\partial d_{001} \cdot 10^3$	5.0	1.0	10.0	5.0 ± 0.1	5.0 ± 0.1	5.0 ± 0.0	5.1 ± 0.1

Table 8: Overview of the means and standard deviations of weight fractions and refined parameters for assemblage 2 using noisy patterns.

<i>Assemblage #2 – Noisy patterns</i>					Multiple specimens (n=50)	Only AD (n=50)	Only EG (n=50)	Only 350°C (n=50)
Phase	Property name	True value	Range		Obtained value $\mu \pm \sigma$	Obtained value $\mu \pm \sigma$	Obtained value $\mu \pm \sigma$	Obtained value $\mu \pm \sigma$
			Min.	Max.				
Illite	wt%	25.0	–	–	25.1 \pm 0.2	25.2 \pm 0.1	25.3 \pm 0.1	24.8 \pm 1.5
	T	13.0	10.0	30.0	13.1 \pm 0.1	13.2 \pm 0.0	12.9 \pm 0.0	13.2 \pm 0.3
Illite/Smectite R0	wt%	25.0	–	–	24.6 \pm 0.4	25.8 \pm 0.2	24.7 \pm 0.1	25.8 \pm 1.9
	T	5.0	3.0	10.0	5.0 \pm 0.1	5.2 \pm 0.0	4.9 \pm 0.0	5.0 \pm 0.4
	Illite content	0.65	0.5	1.0	0.64 \pm 0.01	0.65 \pm 0.00	0.65 \pm 0.00	0.64 \pm 0.04
	2wat / (2wat + 1wat)	0.7	0.0	1.0	0.67 \pm 0.02	0.70 \pm 0.01	–	–
	2 alv / (2alv + 1alv)	0.7	0.0	1.0	0.68 \pm 0.01	–	0.67 \pm 0.00	–
	0 alv / (0alv + 1alv)	1.0	0.8	1.0	0.96 \pm 0.02	–	–	0.96 \pm 0.03
Kaolinite	wt%	12.5	–	–	12.5 \pm 0.0	12.3 \pm 0.0	12.5 \pm 0.0	12.6 \pm 0.1
	T	20.0	10.0	30.0	20.1 \pm 0.1	20.1 \pm 0.0	20.1 \pm 0.0	20.0 \pm 0.0
Kaolinite/Smectite R0	wt%	12.5	–	–	12.8 \pm 0.4	12.1 \pm 0.2	12.4 \pm 0.1	12.5 \pm 0.1
	T	3.0	3.0	10.0	3.0 \pm 0.0	3.0 \pm 0.0	3.0 \pm 0.0	3.0 \pm 0.0
	Kaolinite content	0.80	0.7	1.0	0.80 \pm 0.01	0.81 \pm 0.01	0.81 \pm 0.00	0.82 \pm 0.00
	2wat / (2wat + 1wat)	0.25	0.0	0.6	0.30 \pm 0.11	0.34 \pm 0.03	–	–
	2 alv / (2alv + 1alv)	0.50	0.0	0.6	0.47 \pm 0.10	–	0.54 \pm 0.02	–
	0 alv / (0alv + 1alv)	1.00	0.8	1.0	0.91 \pm 0.05	–	–	0.94 \pm 0.04
Smectite	wt%	20.0	–	–	20.1 \pm 0.2	19.6 \pm 0.2	20.2 \pm 0.1	19.5 \pm 3.4
	T	3.0	3.0	10.0	3.0 \pm 0.0	3.0 \pm 0.0	3.0 \pm 0.0	3.0 \pm 0.2
	2wat / (2wat + 1wat)	0.60	0.5	1.0	0.60 \pm 0.01	0.60 \pm 0.00	–	–
	2 alv / (2alv + 1alv)	0.90	0.5	1.0	0.90 \pm 0.01	–	0.90 \pm 0.00	–
	0 alv / (0alv + 1alv)	0.90	0.8	1.0	0.92 \pm 0.01	–	–	0.91 \pm 0.02
Chlorite	wt%	5.0	–	–	5.0 \pm 0.0	5.1 \pm 0.1	4.9 \pm 0.0	4.9 \pm 0.1
	T	5.0	3	10	5.1 \pm 0.0	5.2 \pm 0.1	5.2 \pm 0.0	5.0 \pm 0.0
	$\partial d_{001} \cdot 10^3$	5.0	1.0	10.0	5.2 \pm 0.3	5.5 \pm 0.3	4.5 \pm 0.2	5.4 \pm 0.3

Table 9: Overview of the means and standard deviations of weight fractions and refined parameters for assemblage 3.

<i>Assemblage #3 – Noisy patterns</i>					Multiple specimens (n=50)	Only AD (n=50)	Only EG (n=50)	Only 350°C (n=50)
Phase	Property name	True value	Range		Obtained value	Obtained value	Obtained value	Obtained value
			Min.	Max.	$\mu \pm \sigma$	$\mu \pm \sigma$	$\mu \pm \sigma$	$\mu \pm \sigma$
Kaolinite	wt%	35.0	–	–	35.0 ± 0.0	35.3 ± 0.6	34.7 ± 0.0	34.9 ± 0.0
	T	18.0	5	40	18.0 ± 0.0	18.0 ± 0.2	18.0 ± 0.0	18.0 ± 0.0
Illite	wt%	30.0	–	–	30.0 ± 0.0	30.0 ± 0.8	30.1 ± 0.1	29.0 ± 0.1
	T	25.0	5	40	25.0 ± 0.0	25.5 ± 0.1	24.8 ± 0.0	25.2 ± 0.12
High-charge smectite	wt%	15.0	–	–	15.1 ± 0.0	16.9 ± 5.9	15.8 ± 0.1	16.0 ± 0.1
	T	10.0	5	40	10.0 ± 0.0	11.3 ± 5.2	10.0 ± 0.0	10.0 ± 0.1
	HC / (HC + LC)	0.90	0.50	1.00	0.90 ± 0.00	0.87 ± 0.06	0.90 ± 0.00	–
Low-charge smectite	wt %	20.0	–	–	19.9 ± 0.0	17.8 ± 7.2	19.4 ± 0.2	20.3 ± 0.2
	T	10.0	5	40	10.0 ± 0.0	12.2 ± 7.4	10.0 ± 0.0	10.2 ± 0.1
	LC / (LC + HC)	0.80	0.50	1.00	0.80 ± 0.00	0.83 ± 0.06	0.80 ± 0.00	–

Table 10: Overview of the means and standard deviations of weight fractions and refined parameters for assemblage 4.

<i>Assemblage #4 – Noisy patterns</i>					Multiple specimens (n=50)	Only AD (n=50)	Only EG (n=50)	Only 350°C (n=50)
Phase	Property name	True value	Range		Obtained value	Obtained value	Obtained value	Obtained value
			Min.	Max.	$\mu \pm \sigma$	$\mu \pm \sigma$	$\mu \pm \sigma$	$\mu \pm \sigma$
Kaolinite	wt%	50.0	–	–	49.7 \pm 0.1	49.3 \pm 0.0	50.3 \pm 0.2	49.3 \pm 0.1
	T	15.8	5	40	15.2 \pm 0.1	15.2 \pm 0.0	15.2 \pm 0.0	15.6 \pm 0.0
Illite	wt%	50.0	–	–	50.3 \pm 0.1	50.7 \pm 0.0	49.7 \pm 0.2	50.7 \pm 0.1
	T	30.0	5	40	21.2 \pm 0.0	18.8 \pm 0.0	22.7 \pm 0.1	28.0 \pm 0.0
	Oct. Fe ³⁺ / Oct. Al ³⁺	0.125	0	0.5	0.133 \pm 0.000	0.126 \pm 0.002	0.151 \pm 0.001	0.139 \pm 0.001
	K content	1.50	0	2	1.52 \pm 0.01	1.49 \pm 0.00	1.52 \pm 0.01	1.44 \pm 0.00

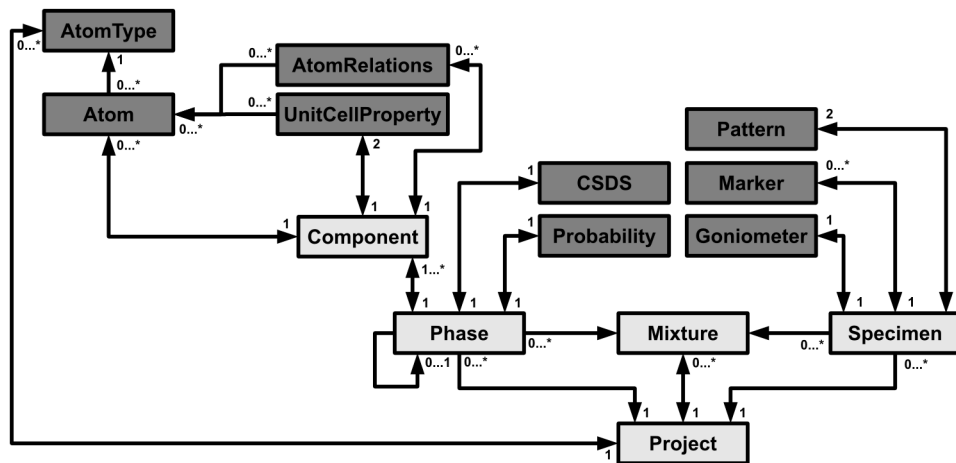


Figure 1: Schematic overview of the most important objects in PyXRD and their relations. Arrows indicate 'is referenced x times by' relations and the numbers indicate the multiplicity of that relation (e.g. Project holds 0 or more references to AtomType).

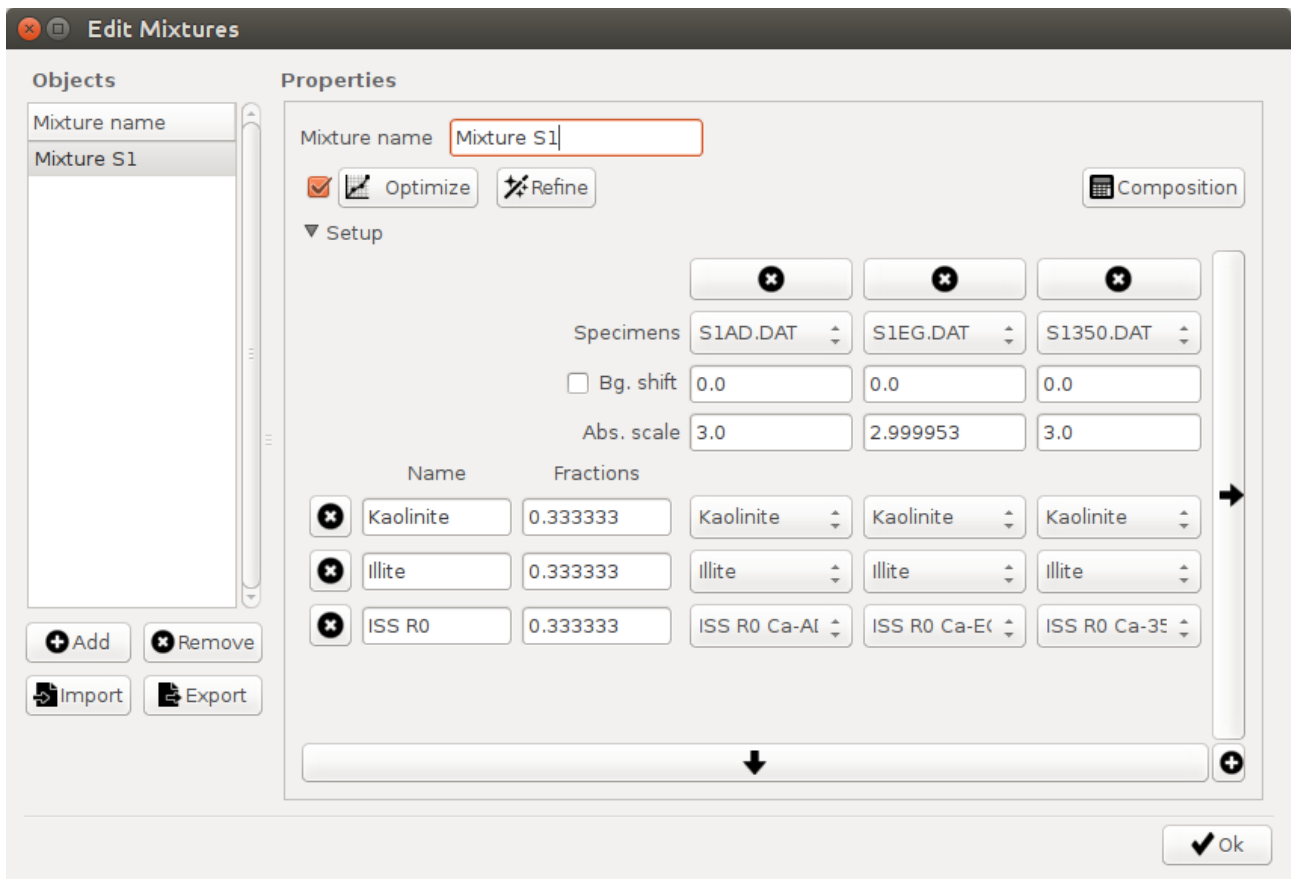


Figure 2: screenshot showing the 'Edit mixtures' dialog where a user can link different phases (Kaolinite, Illite, ISS R0 Ca-AD, ...) with the corresponding specimens (S1AD.dat, S1EG.dat, ...).

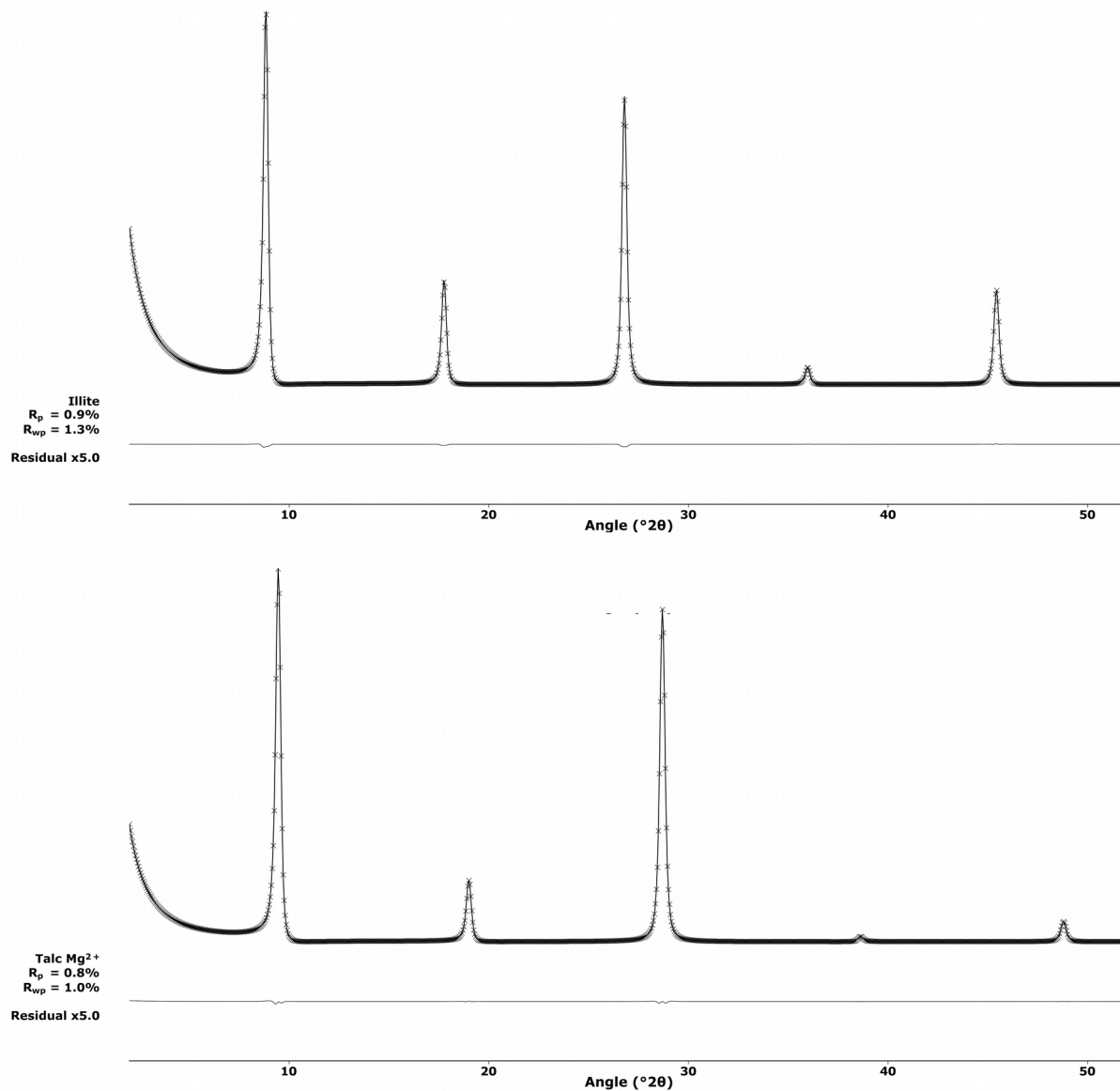


Figure 3 – Calculated patterns for discrete illite (top) and talc (bottom), showing nearly identical output for PyXRD (solid line) and Sybilla (crosses). For clarity the residual patterns are scaled to 5x their original intensity.

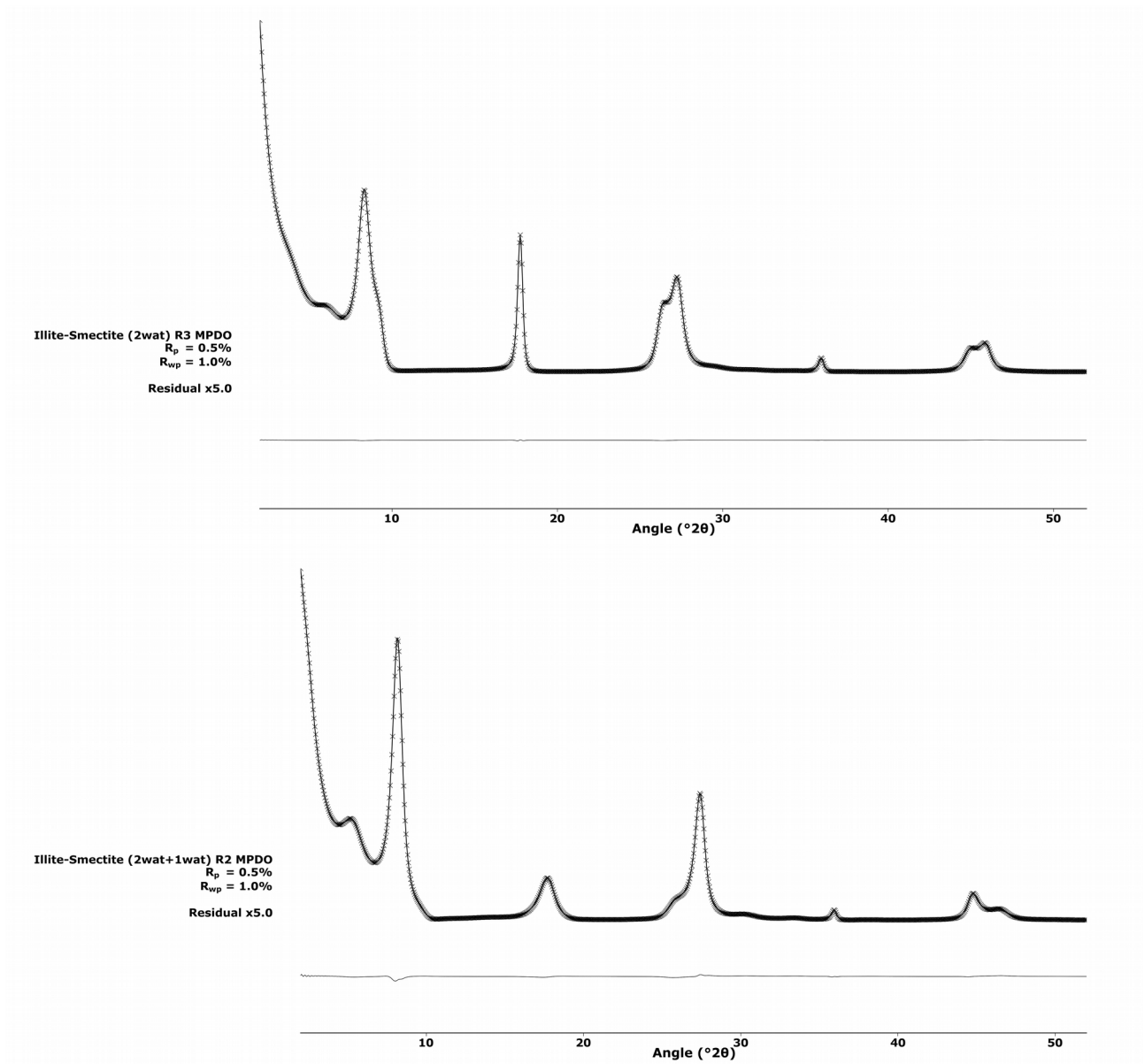


Figure 4 – Calculated patterns for illite-smectite (IS) R3 (top) and illite-smectite (ISS) R2 (bottom; both have MPDO), showing nearly identical output for PyXRD (solid line) and Sybilla (crosses). For clarity the residual patterns are scaled to 5x their original intensity.

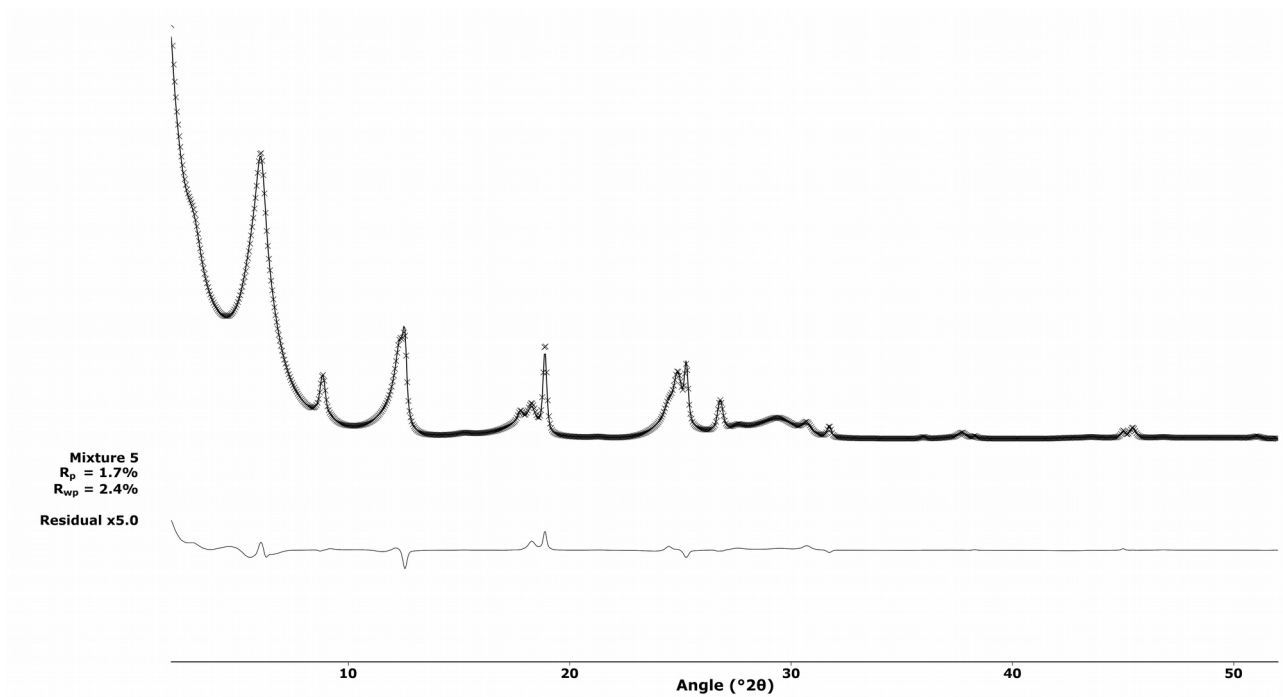


Figure 5 – Calculated patterns for mixture 5 for PyXRD (solid line) and Sybilla (crosses). For clarity the residual pattern is scaled to 5x its original intensity.

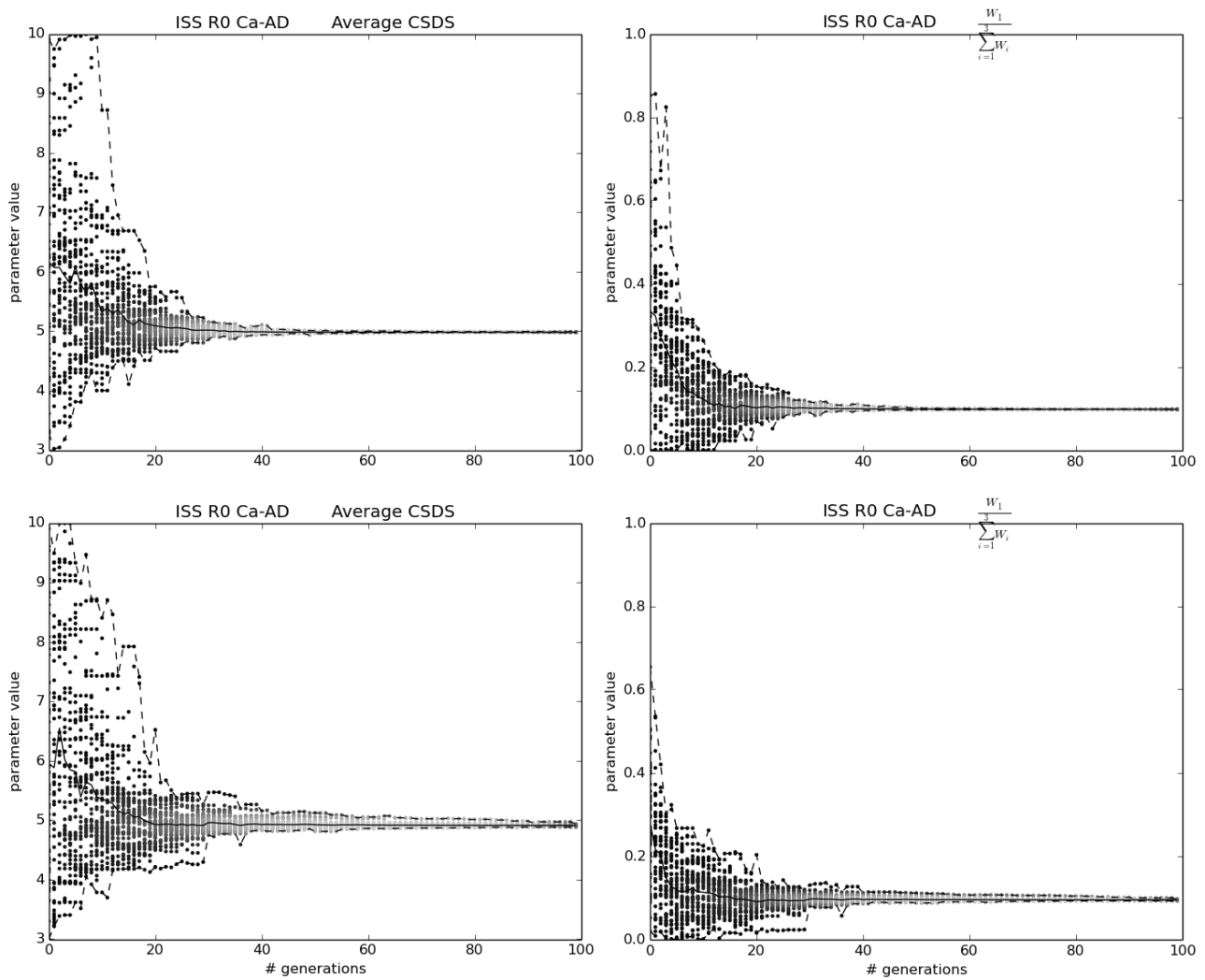


Figure 6: Parameter evolution plots (left: average CSDS; right: illite content) for the noisy patterns of assemblage 1 for the multispecimen run (top plots) and the isolated AD run (bottom plots). Minimum and maximum values during the refinement are indicated with dashed lines, iterations' best solutions at each generation indicated by dots and average solution with a solid line. The higher the density of the dots, the lighter they are colored.

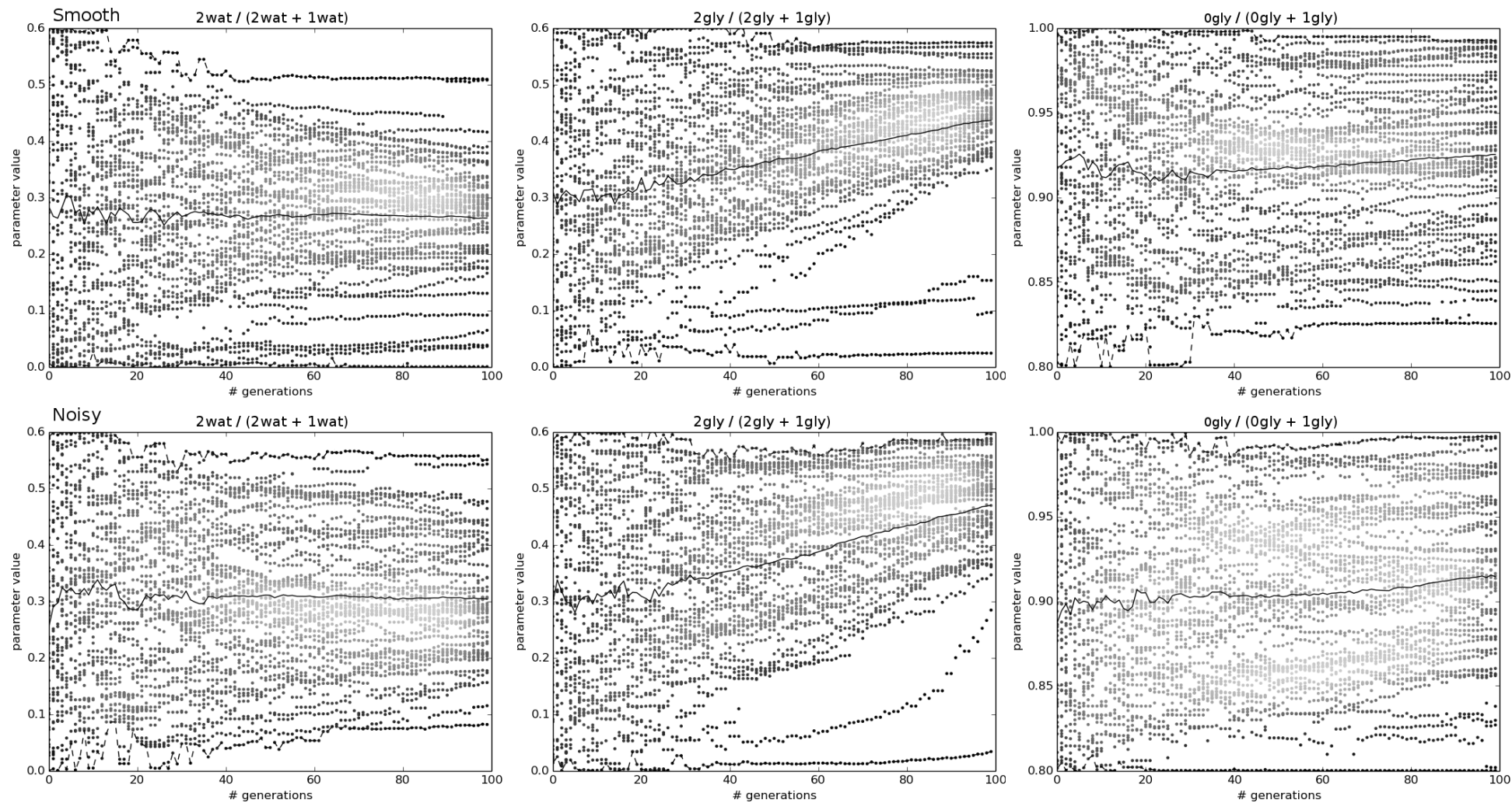


Figure 7: Parameter evolution plots for the smectite fractions in the kaolinite-smectite mixed layer of assemblage 2 using the multispecimen setup. Plots for the smooth patterns are in the top row, for noisy patterns in the bottom row. Legend as in Figure 6.

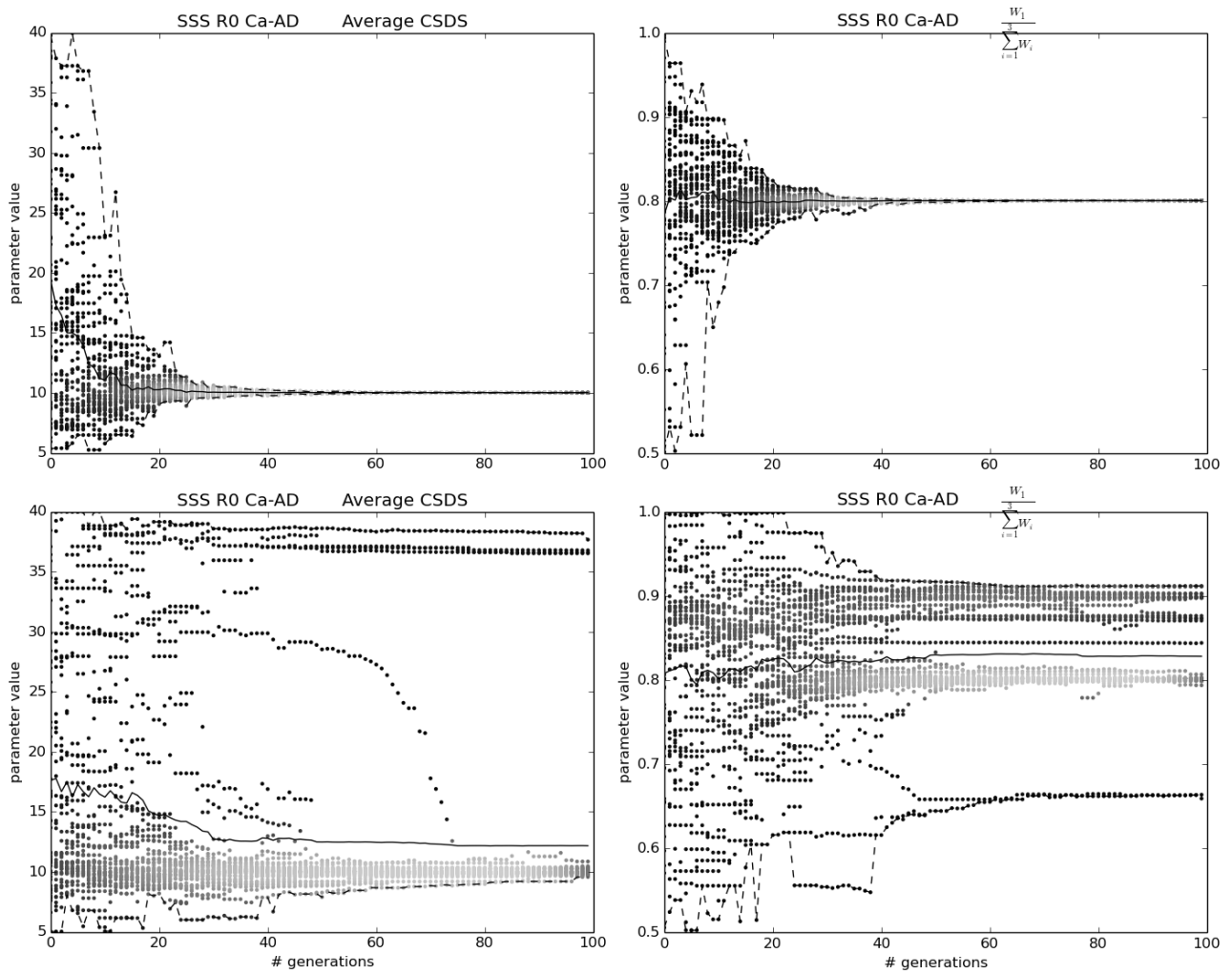


Figure 8: Parameter evolution plots for the low-charge smectite in assemblage 3. Plots for the multispecimen setup are in the top row, for the AD single pattern setup in the bottom row. Legend as in Figure 6.

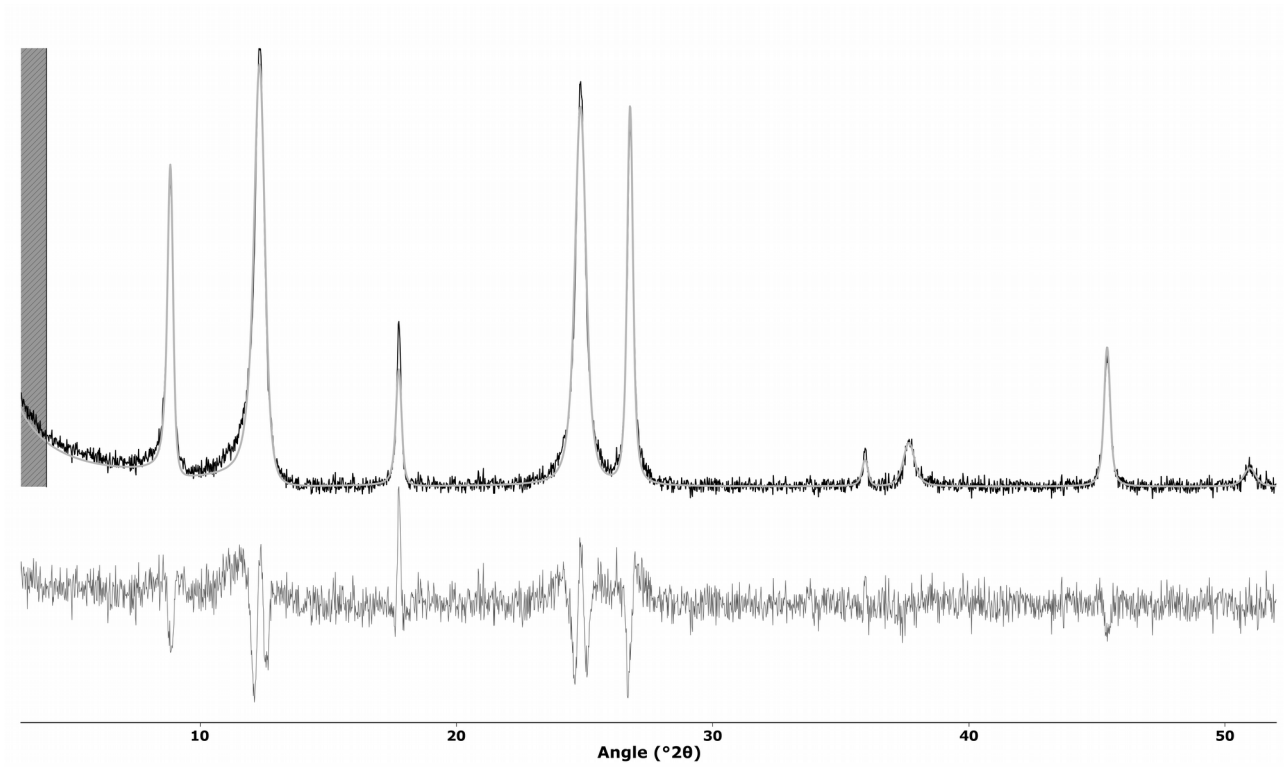


Figure 9: The input (black solid line) and refined (grey solid line) AD pattern and their difference (grey solid line at the bottom) for the multispecimen setup of assemblage 4. An observant user should see the mismatches in the patterns and realize his model needs improvement.